Constitutive behaviour of masonry prisms using a full-field measurement technique

Ismail Bello[1, 2, *], George Wardeh [1], Belén González-Fonteboa [2], Fernando Martínez-Abella[2], Elhem Ghorbel[1]

1. PhD Candidate, Department of Civil engineering, CY Cergy Paris University, 95000 Neuville-sur-Oise, France

1. Associate Professor, Department of Civil engineering, CY Cergy Paris University, 95000 Neuville-sur-Oise, France

2. Associate Professor, Department of Construction Technology, University of A Coruna, 15008 Coruna, Spain

2. Full Professor, Department of Construction Technology, University of A Coruna, 15008 Coruna, Spain

[*]Corresponding author email: ismail.bello@cyu.fr

Abstract

To obtain analytical models for the compressive behaviour of masonry structures, it is crucial to accurately measure the compressive strengths of its constituents, i.e., brick and mortar. The mechanical properties and the stress-strain relationship under uniaxial compression are essential for thoroughly investigating and evaluating masonry structures. The present work aims to validate a non-contact measuring technique for obtaining full-scale strain and failure patterns and investigate joint mortar composition's effect on masonry behaviour. Forty masonry prisms were manufactured in this study using two distinct types of brick and five different types of mortar varying according to cement and lime contents. The results showed that 2D Digital Image Correlation (DIC) could generate full-strain assessments of masonry prisms, resulting in a full-scale stress-strain analysis. It was also found that, in the post-peak region, prisms with lower cement content exhibit a more ductile behaviour with strain localisation at the joint mortar level. Based on current experimental results and data from the literature, new analytical relationships were presented to predict masonry mechanical properties and masonry complete stress-strain compressive behaviour.

Keywords: Digital image correlation (DIC), Mechanical properties, Masonry, Compressive strength, Analytical model, Stress-Strain law.

1. Introduction

Historical structures often use stone, rock blocks, and baked clay bricks as their primary building materials and masonry mortars as binders[1]. The overall performance is determined by the volume fraction of the two parts, the interactions between them and the joint mortar's strength [2].

Non-hydraulic lime, hydraulic lime, cement, pozzolans, and clay are standard binders in monumental structures [3]. Non-hydraulic lime mortars harden by reactivity with carbon dioxide, whereas hydraulic lime mortars set and harden by reaction with water. The calcium silicate content and the hydraulicity level of natural hydraulic limes determine the strength class of the material [4]. Masonry's behaviour under uniaxial compression has been investigated by [5–12], and it has been demonstrated that the elastic modulus (E_m), strain at peak stress (ε_m), and compressive strength of the masonry (f_m) are all influenced by the properties of brick and mortar. The aforementioned masonry parameters can be predicted from the compressive strength of brick and mortar using the mathematical techniques provided by Eurocode 6 [13] and numerous studies [5,10,14–25].

The constitutive stress-strain law under uniaxial compressive loading is the primary input data for analysing full-scale masonry structures, especially for numerical models. The typical stress-strain relationship proposed by [13] is non-linear and can be modelled using a parable with an ascending branch up to the ε_m. For the post-peak phase, the standard [13] authorises taking a horizontal plateau or a descending branch up to an ultimate strain equal to 0.0035. Kaushik et al. [10] adapted the same model as Eurocode 6 for the pre-peak phase and up to the strain corresponding to 90% of the f_m in the descending branch. Beyond this strain, the researchers proposed a linear relationship up to an ultimate strain equal to $2\varepsilon_m$ or $2.5\varepsilon_m$, depending on the mortar type (with or without lime). Ewing and Kowalsky [26] also adopted the same methodology. More recently, Yang et al. [11]used the general form of the model proposed by Carreira and Chu [27] for concrete. According to this model, a simple non-linear equation allows the modelling of the entire stress-

strain curve. However, no control points are proposed in the post-peak branch, which is crucial for curve adjustments to reproduce experimental data. This leads to an overestimation of the post-peak strains

The above researchers have tried to calibrate the models using their results and some data from the literature; however, the number of data remains limited to validate a model. In addition, the experimental measurement of strains is done using a point-wise technique (strain gauges and Linear Variable Differential Transformers (LVDTs)); hence not reliable for post-peak behaviours. In that regard, full-field measurement techniques such as Digital Image Correlation (DIC) are usually preferred for the full-scale characterisation of the behaviour of masonry structures.

A comprehensive review of Two Dimensions (2D) DIC measurement is provided by Pan et al. [28]. In most studies, the region of interest is limited to a small portion of the specimen, and only in-plane measurements can be correctly analysed. DIC analysis was used to map crack evolution in masonry walls [29], investigate the influence of service loads on crack development [30], and study the masonry stress-strain behaviour under loading-unloading conditions[31]. Tung et al. [32] conducted load tests on a small masonry wall oriented at an angle of 45 degrees using DIC to analyse the deformations and cracks formed on the wall's surface. However, the possibility of incorporating this technique to study strain localisation and the constitutive law of masonry has not been widely discussed in the literature.

The need for a full, characteristic prediction model applicable to higher f_m with varied mortar compositions (lime, cement, and lime-cement) is yet to be thoroughly investigated. Due to a lack of experimental data that appropriately considers the plastic behaviour of masonry, it is difficult to model the behaviour of masonry structures accurately.

The present work adopts the DIC technique to measure the displacement and strain analysis during the monotonic compressive tests on masonry prisms. Analytical models are proposed using current experimental results and 478 experimental data points from the literature to estimate the masonry mechanical properties. A simplified non-linear stress-strain model is also proposed to predict the full behaviour of masonry under uniaxial compression, considering different mortar compositions.

2. Materials and experimental procedure

2. 1 Test samples

Two non-hollow masonry-fired clay bricks named B1 and B2 with five different laboratory-designed mortar mixes (Figure1) were used to construct the masonry prisms. The physical properties of both fired bricks are given in Table 1.

Table 1 Physical properties

Specimen	Density (kg/m^3)	Water absorption (%)	Porosity (%)
Brick 1 (B1)	2.00	9.54	19.37
Brick 2 (B2)	1.88	7.77	14.58

The laboratory mortars were prepared following the standard EN-P18-452 [33] using Portland cement CEM I 52.5 N CE CP2 NF and hydraulic lime EN 459-1 NHL 5 as binder constituents with a sand particle distribution of 0-2 mm. All samples stayed for 24 hours in Acrylonitrile Butadiene Styrene (ABS) plastic moulds and were later removed and immersed in water, maintained at room temperature for 28 days. The water to binder ratio had values of 0.55, 0.65 and 0.7. The mixture compositions of laboratory mortars are summarised in Table 2.

Table 2. Mix proportions of joint mortars

Components (kg/m^3)	Mortars' compositions				
	Mortar-M1	Mortar-M2	Mortar-M3	Mortar-M4	Mortar-M5
Cement	500	350	250	150	0
Lime	0	150	250	350	500
Water	275	325	350	350	350
Sand	1387	1336	1132	1312	1312
Lime/Cement	0	0.42	0.5	2.3	-
W/B ratio	0.55	0.65	0.7	0.7	0.7

Forty masonry prisms with a 10-16 mm joint thickness were prepared following the procedure reported by Sarangapani et al. [34]. The brick units were first submerged in water for two minutes before laying to reduce the mortar shrinkage effect during the curing process and enhance the brick–mortar bond adherence. B1 and B2 brick units were used to construct two series of masonry prism, namely (MP1) and (MP2), respectively. A bond stack of five bricks was built for each masonry prism, making an average height of 314 mm for MP1 and 364 mm for MP2. An aluminium formwork and a bubble level were used during the construction to ensure the

specimens' verticality and horizontality. After construction, the masonry prisms were covered with humid clothes and polythene bags for 28 days in a laboratory environment (Figure 2).

B1 and B2 units were wire-cut into small beams using a mechanical saw for flexural testing. For compressive tests, both brick and mortar specimens were cut to a volume of 40x40x40 mm^3. All prisms were tested under compressive monotonic loading to attain their entire material behaviour. Table 3 regroups the characteristics of all used materials and constructed masonry prisms with the executed mechanical tests.

Table 3. Specimen characteristics and test specification. B: Fired clay brick; M: Masonry mortar (Cement, Lime, and River sand); MP: Masonry prism (Fired clay brick and masonry mortar)

Specimen	Dimension (mm^3)	Test Type	Number of tested specimens
B1 and B2	40x40x160	3-point Flexural test	12
	40x40x40	Compressive test	24
M1, M2, M3, M4 and M5	40x40x160	3-point Flexural test	15
	40x40x40	Compressive test	30
MP1	50x100x220	Compressive test	20
MP2	60x110x230		20

a) b)

Figure 1. Constituents of Masonry Prism a) Masonry mortar b) Prismatic bricks.

a) b)

Figure 2. Masonry Prisms a) Prisms during construction. b) Prisms during curing

For the 2D DIC measurements on MP1 and MP2, a plane surface was chosen as the Surface Of Interest (SOI), and then the SOI was checked for roughness and smoothened with an electric sander where necessary. White paint was applied to the SOI with zero thickness. Subsequently, a matte black spray was applied stochastically to give the desired speckle pattern on all the specimens [35]. To assure the repeatability of the DIC protocol, two uniaxial polyimide material strain gauges of 120 ohms with a length of 30 mm, were glued to each masonry specimen's mid-height opposite and parallel to the axis of loading of masonry prisms (Figure 3).

a) b) c)

Figure 3. Prisms a) Specimen prepared for DIC b) Speckle Pattern applied on SOI c). Strain gauges on the opposite surface.

2. 2 Experimental apparatus and setup

For mortar and brick units, flexural and compressive tests were conducted on a 3R Instron machine, loading at a rate of 0.1 mm/min and 0.5 mm/min for flexural and compressive testing, respectively. The same brick face has been maintained for all test experiments on bricks and masonry prisms. The masonry prisms' tests were conducted using a 2-column frame Schenck machine capable of applying a maximum load of 3000 kN and regulated at 0.5 mm/min. The experimental setup can be visualised in Figure 4.

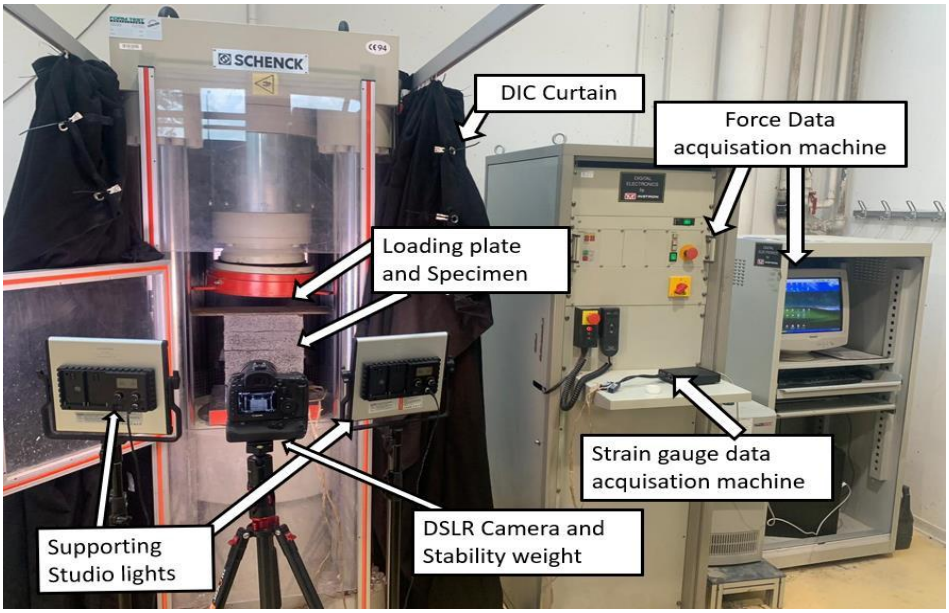

Figure 4 Experimental setup for masonry Prism

Before the testing, particular care was taken to ensure the centrically placing of every specimen and symmetrical positioning of the loading set. Masonry prisms' loading surfaces were sandpapered to ensure perfect horizontality to the machine's loading plates, and strain gauges were relayed to an acquisition system and checked for any errors before starting the test.

Images for 2D DIC were taken using a 5D Canon Mark IV digital camera with 6720 x 4480 pixels and a focal length of 25-70 mm (EF f/2.8L II USM). The camera was placed on a tripod and distanced at 1.3m away from the specimen with a mass attached to the tripod to retain stability. Two professional studio lights provided adequate brightness, and then a black curtain was used to cover the experimental setup to maintain constant illumination throughout the test. The camera's optical axis was directed perpendicular to the SOI of the specimen using a laser beam, while the

camera's exposure and other settings were kept constant all through the experiment. The camera sensor sensitivity was adjusted to ensure sufficient photo brightness with minimum noise output at ISO 800, and it was controlled by a measuring rate of two frames per second (fps). All sets were in manual mode to ensure continuity and avoid changes throughout the test. Finally, each DIC test was started from a distanced remote control to prevent disturbance of the configuration.

2. 3 Image Post Processing

Image processing was done using GOM correlate 2D [36], a free 2D DIC commercial software capable of measuring full-field displacements and deformations of in-plane motion. In GOM, the captured surface is divided into subsets, and all subsets have a different random pattern achieved by the stochastic pattern. To compare DIC and strain gauges results, 30 mm virtual extensometers were defined in the same positions as strain gauges on the SOI. However, one of the evaluation difficulties was selecting appropriate representative measuring points on the SOI, which are visible throughout the test procedure because surface detachment was noticed in some specimens (Figure 5).

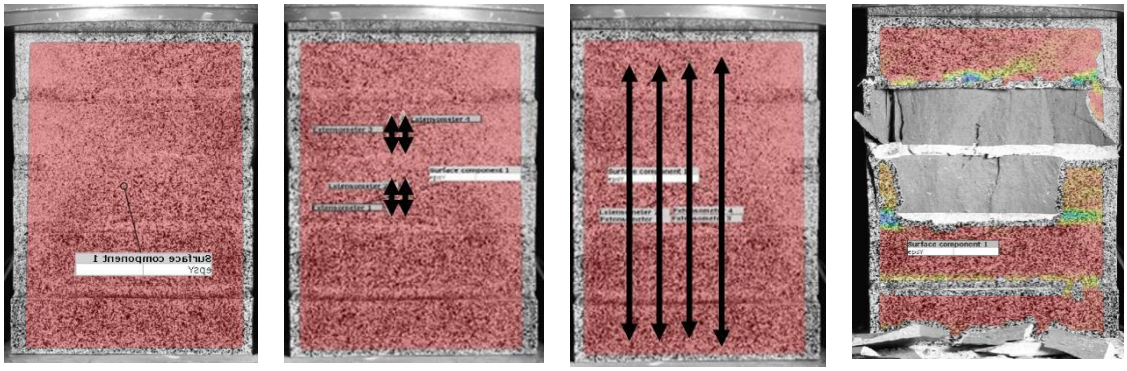

a) b) c) d)

Figure 5 Specification of Prism SOI, a) SOI of a prism, b) Prism with 30 mm virtual extensometers, c) Prism with 314 mm virtual extensometers, c) Prism at peak load.

3. Results and discussion

3. 1 Brick and mortar units

Table 4 recapitulates the average mechanical properties of bricks and joint mortars with their Coefficient Of Variation (C.O.V). It can be observed that the compressive strength of B1 is twice as high as that of B2, while its flexural strength of B1 is three times higher than B2. Concerning

the mortars, the compressive and flexural strengths decrease with the increase in the lime content of specimens.

Table 4 Mean and standard deviation results of Fired clay samples and mortar

Units	Fired clay		Mortar				
Specimen	B1	B2	M1	M2	M3	M4	M5
Compressive strength (MPa)	90.01	37.73	49.26	39.30	21.57	16.55	3.50
C.O.V (%)	3.30	1.39	5.60	0.93	0.57	0.05	0.5
Flexural strength (MPa)	5.07	1.53	3.67	3.39	2.87	1.91	0.83
C.O.V (%)	0.10	0.55	0.30	0.24	0.26	0.09	0.75

3. 2 Masonry Prisms

Masonry prisms were designated using the abbreviation MPi-Mj, where "i" refers to the brick type (1 or 2), and "j" refers to the joint mortar (1, 2, 3, 4 or 5).

The overall mechanical properties of prisms in this work are regrouped in Table 5. The properties involves f_m, ε_m, E_m, and also recapitulates the brick strain at the prism's peak load obtained by the DIC technique and strain gauges, respectively ε_{B-DIC} and ε_{B-SG}.

The (ε_m) and (E_m) were obtained from DIC full-field measurement. The E_m was measured within 5-33% of the f_m [13].

Table 5 shows that the masonry f_m depends on the compressive strength of brick, f_b as well as the compressive strength of the joint, f_j. As the B1 is more resistant than B2, the MP1 prisms have higher f_m than MP2 prisms for the same type of joint mortar.

The brick unit properties were compared to validate the DIC technique at the scale of masonry prisms. The results show they correspond well regarding strains between the strain gauges and DIC, except for MP1-M1.

Table 5 Mechanical properties of masonry.

Specimen	Masonry						Brick			
	f_m (MPa)		ε_m (‰)		E_m (GPa)		ε_{B-SG}(‰)		ε_{B-DIC}(‰)	
	Average	C.O.V (%)	Average	C.O.V (%)	Average	C.O.V (%)	Average	C.O.V (%)	Average	C.O.V (%)
MP1-M1	37.07	2.52	1.93	10.30	20.14	10.85	0.83	18.02	1.10	15.05
MP1-M2	33.92	2.14	3.00	11.78	14.92	8.46	1.82	5.29	1.59	8.92
MP1-M3	29.39	6.33	3.94	6.83	8.10	5.54	1.23	2.35	1.25	3.23
MP1-M4	23.52	12.19	3.47	10.66	8.79	18.06	1.41	5.52	1.43	9.82
MP1-M5	18.30	7.54	7.88	3.90	2.69	8.45	1.01	10.51	1.10	2.59
MP2-M1	22.36	9.14	2.98	5.33	11.27	8.21	1.52	2.23	1.49	12.67
MP2-M2	19.46	7.64	3.37	7.47	5.33	16.24	1.11	3.50	1.20	7.52
MP2-M3	17.76	8.35	2.74	17.97	12.51	16.35	1.23	5.80	1.28	2.34
MP2-M4	16.77	7.11	5.41	6.72	8.88	7.21	1.85	11.2	1.67	13.57
MP2-M5	14.32	8.33	5.28	15.98	4.53	16.93	1.23	4.29	1.28	3.98

3. 3 Stress-strain relationship masonry prisms

Figure 6 regroups the stress-strain curves for the MP1 series, and the strain measurement obtained for brick units B1 using the DIC technique and strain gauges. It is worth mentioning that DIC results were obtained using virtual extensometers placed at the same position, as shown in Figure 5. b, 5, c.

Both techniques gave similar trends at the brick level except for prisms MP1-M1 and MP1-M2 constructed with high cement content mortar joints. All masonry prisms show a linear behaviour up to approximately 70% of the f_m. Materials with high f_m show a brittle post-peak behaviour (Figures 6. a-6. c), while other samples show more ductile descending branches (Figures 6. d-6. e).

Figure 7 illustrates the stress-strain curves for the MP2 series constructed with the brick B2. It can be shown that all prisms show a linear behaviour until 70% of f_m. As for the MP2 series, the post-cracking behaviour depends on the joint performance. The weaker the joint, the more ductility the prism shows at the descending branch.

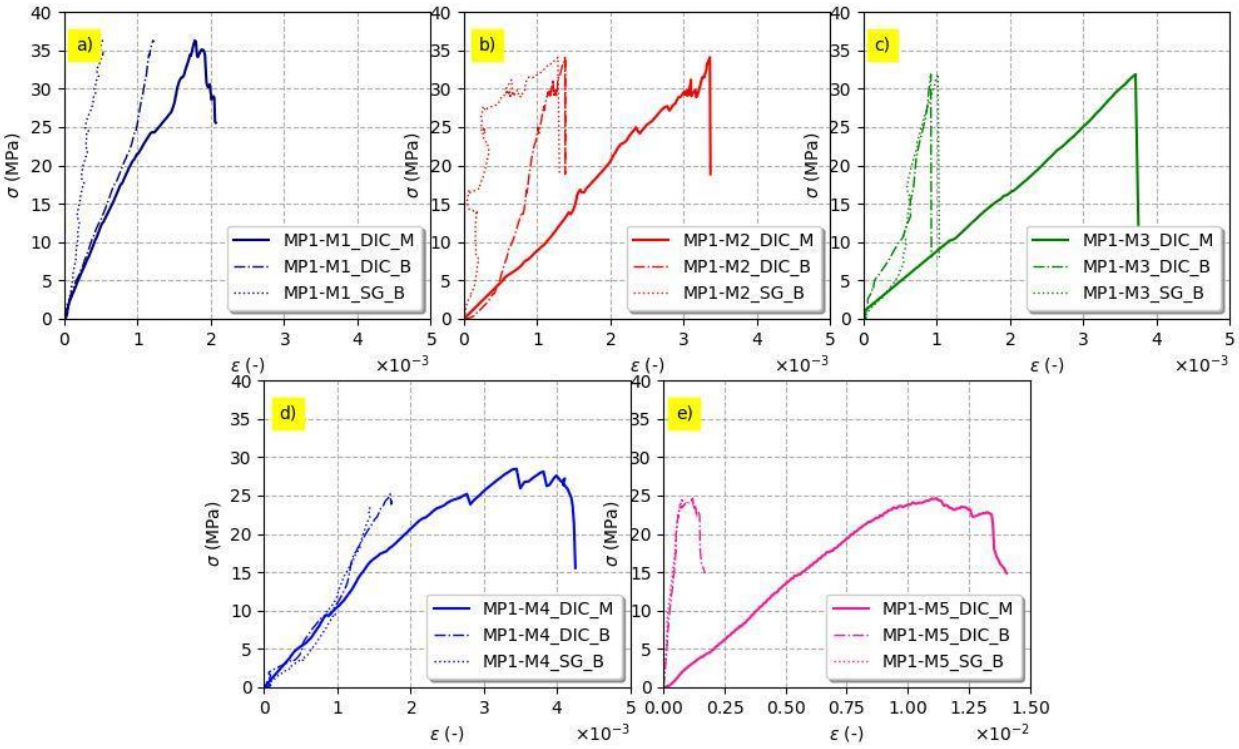

Figure 6 MP1 stress-strain curves a) MP1-M1. b) MP1-M2. c) MP1-M3. d) MP1-M4. e) MP1-M5.

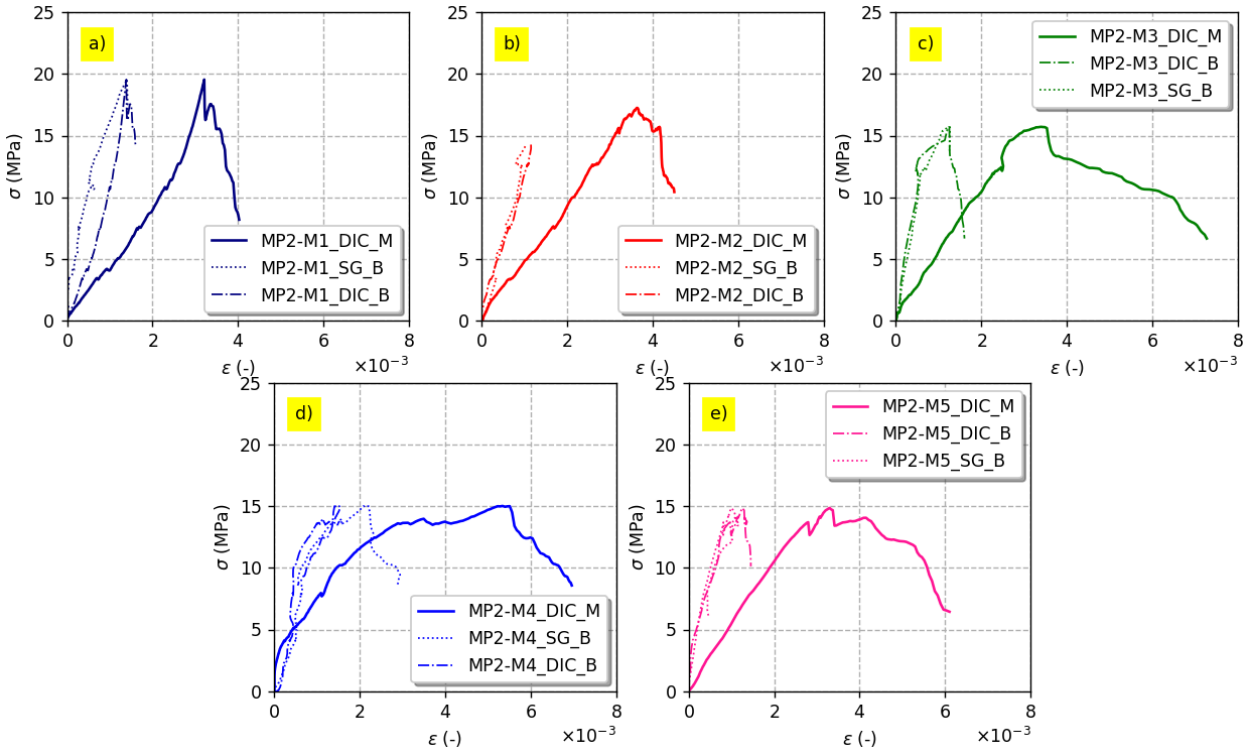

Figure 7 MP2 stress-strain curves a) MP2-M1. b) MP2-M2. c) MP2-M3. d) MP2-M4. e) MP2-M5*.

* DIC_M stands for the result from the virtual extensometer defined on the entire length of the masonry prism, _DIC_B stands for the result obtained from the 30 mm virtual extensometer defined on brick, and _SG_B stands for the result obtained from the 30 mm strain gauge glued on brick.

3. 4 Failure pattern

With 2D DIC, strain evolution was followed until the total failure of the SOI. The collapse is influenced primarily by the composition of the mortar than the brick. Figure 8 shows the SOI of tested prisms at the maximum loading with corresponding strain visualisation. Three types of failure patterns are noticed. For prisms with high cement content (MP1-M1, MP1-M2, MP2-M1, MP2-M2), in subfigures 8. a, 8. b, 8. f, and 8. g, strains accumulate on bricks, then propagation of random vertical cracks on prism (wide and narrow face) and spalling of the brick surface. These cracks grow rapidly, causing a brittle failure with an explosive sound. For prisms with equal binder contents (MP1-MP3, MP2-MP3), in subfigures 8. c and 8. h, strain localisation is noticed at the joints, with fewer vertical crack propagation on bricks, then spalling of parts of the SOI. Thereby, prisms with high lime content (MP1-M4, MP1-M5, MP2-M4, MP2-M5), in Figures 8. d, 8. e, 8. i and 8. j show a more ductile behaviour, having almost equal strain localisation at the mortar joints with little or no cracks on prisms after the test. A similar failure pattern was reported by McNary, and Abrams [6].

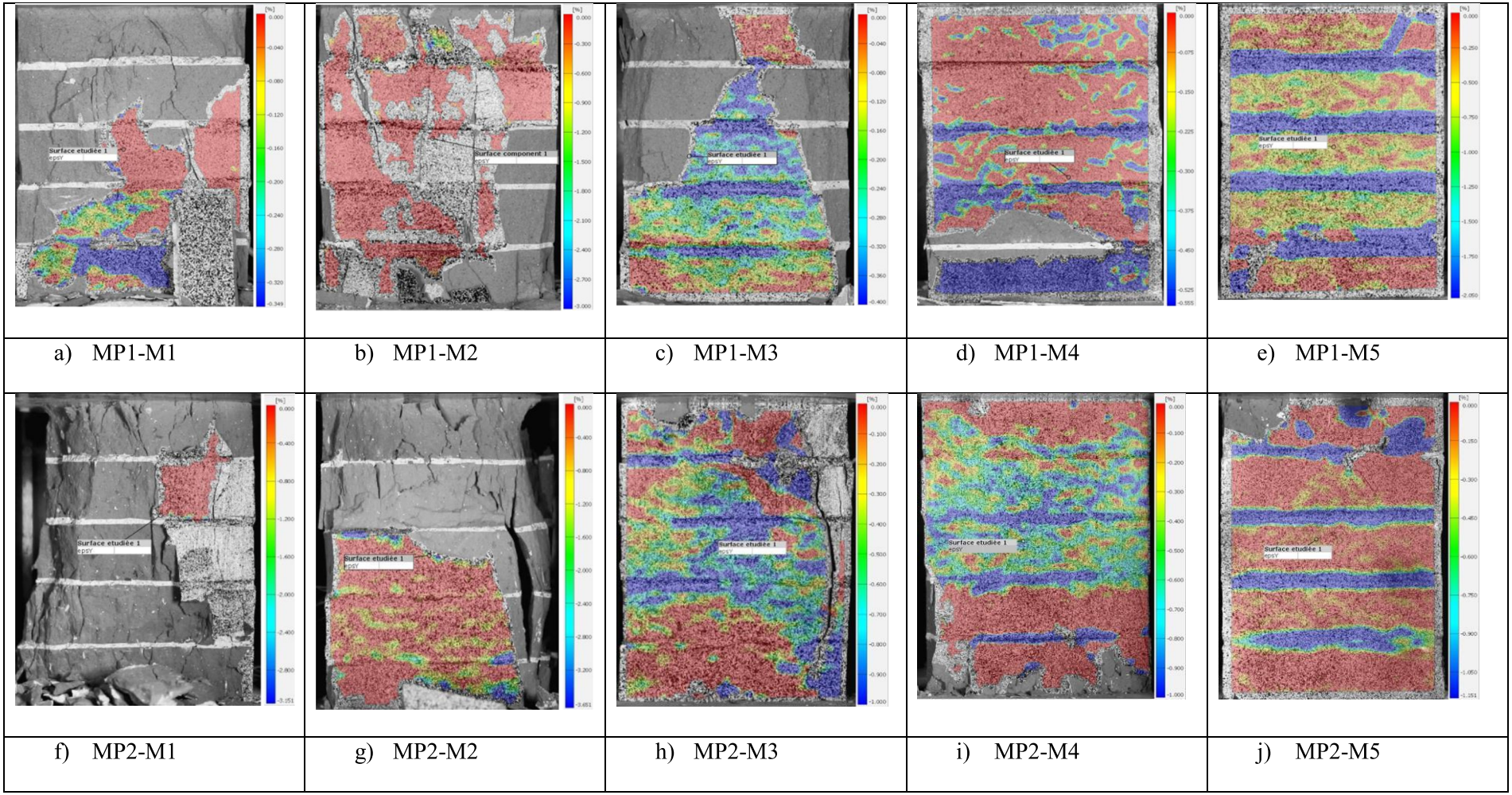

a) MP1-M1	b) MP1-M2	c) MP1-M3	d) MP1-M4	e) MP1-M5
f) MP2-M1	g) MP2-M2	h) MP2-M3	i) MP2-M4	j) MP2-M5

Figure 8 Strain visualisation at maximum stress on masonry prisms

4. Analytical modelling

4. 1 Prediction of mechanical properties

The masonry's compressive strength, $f_{m,}$ is the fundamental property used in the design standards to assess the performance of masonry structures [10,37]. It is also used to estimate the E_m and the ε_m. A reasonable prediction of the stress-strain relationship becomes possible when these parameters are correctly estimated, especially if it is difficult to conduct experimental tests.

The results of the present work with other 478 experimental data were taken from the references [5–11,21,24,37–40]. They were used to verify the validity of the proposed analytical models and confirm the reliability of obtained results employing 2D DIC. The details of the entire database are given in Table 6.

It was reported in the literature that f_m depends on the f_b and f_j [5,6,10,25]. The mathematical expression that connects the three properties is written in the form:

$$f_m = k f_b^{\alpha} f_j^{\beta} \qquad (1)$$

where k, α and β are constants found by regression analysis. Eleven analytical models were verified using 221 data points before proposing a new expression that better fits the experimental results for the estimation of f_m. For each tested model, the ratio between the experimental mean value and the mean of the predicted value was calculated in addition to the standard deviation, the variance, and the coefficient of determination between the experimental and predicted values named R^2. Table 7 shows that the available analytical relationships do not allow a satisfactory prediction of the f_m. In the present study k, α and β were refitted using a similar methodology as [13]. The proposed model, expressed by equation 2, gives the best determination coefficient R^2 and the closest ratio between the experimental mean value and the mean predicted value (Table 7).

$$\begin{aligned} f_m &= 0.09 f_b^{0.32} f_j^{1.22} \quad f_b \leq 20MPa \\ f_m &= 1.90 f_b^{0.06} f_j^{0.79} \quad f_b > 20MPa \end{aligned} \qquad (2)$$

The relationship between the E_m and the f_m, is proposed in masonry standards and some references in the form:

$$E_m = k f_m \qquad (3)$$

where k represents a constant that varies between the references.

The validity of six models of the form given by equation 3 was verified with 147 experimental values, and the results are shown in Table 8. It can be observed that four of these models gives a negative correlation factor of R^2, meaning that the predicted values do not agree with the experimental data. In this study, a new analytical expression was proposed (Equation 4):

$$E_m(MPa) = 320 f_b^{0.63} f_j^{0.23} \quad (4)$$

The proposed equation fits the experimental results with a correlation factor $R^2 = 0.54$, which is the highest compared to all the models evaluated.

The ε_m can be estimated according to the general form given by Equation 5, although other forms can be found in the literature [11,24].

$$\varepsilon_m = \frac{A f_m}{f_j^{\gamma} E_m^{\xi}} \quad (5)$$

with A, γ and ξ constants found by linear regression. Using 131 experimental points, several models [5,10,11,24,25] were verified for predicting ε_m. The results recapitulated in Table 9 show that most of these models are not adequate to predict ε_m where the correlation coefficient is lower than zero, while the reliability level of the other tested models is low. For this reason, the parameter of Equation 5 was refitted, and a new expression is proposed in Equation 6, which allows a better estimation of ε_m with a correlation factor $R^2 = 0.79$.

$$\varepsilon_m = \frac{0.48 f_m}{f_j^{0.06} E_m^{0.84}} \quad (6)$$

The predicted versus experimental values using Equations 2, 4 and 6 are depicted in Figure 9.

Table 6 Literature studies used in the database

Reference	Type of units	Constituents of Mortar			Number of tested specimens	Number of datasets	f_b (MPa)	f_j (MPa)	f_m (MPa)	E_m (MPa)	ε_m
		Cement	Hydraulic Lime	River sand							
Present Author	Fired clay bricks	✓	✓	✓	40	40	37.73 - 90	3.5 - 49.3	14.2 – 38.37	2500 - 22660	0.0018 - 0.0083
Lumantarna et al. [5]	Vintage fired clay bricks	✓	✓	✓	120	22	8.5 - 43.4	0.69 - 23.2	3.31 - 30.79	388 - 7971	0.0028 - 0.0143
McNary and Abrams [6]	Fired clay bricks	✓	✓	✓	16	4	101.7	3.4 - 52.6	29.8 - 48.1	12699 - 15320	0.0033 - 0.0045
Domede et al. [38]	Burnt clay bricks	×	✓	✓	12	6	11.5 - 17.57	3.16 - 3.98	6.1 - 10.8	4737 - 5991	0.0041 - 0.010
Thaickavil and Thomas [9]	Fired clay bricks	✓	×	✓	48	16	6.7	13.6 - 35.5	1.22 - 3.15	-	-
Aref and Dolatshahi [39]	Fired clay bricks	×	✓	✓	7	7	13.5 - 41	13.8	10.0 - 35.1	4300 - 4585	0.0038 - 0.017
Kaushik et al.zzz [10]	Fired clay bricks	✓	×	✓	84	12	16.1 - 28.9	3.1 - 20.6	2.9 - 8.5	1795 - 5219	0.0028 - 0.004
Thamboo and Dhanasekar [24]	Fired clay bricks	✓	×	✓	50	10	3.8 - 15.8	3.98 - 6.46	1.36 - 7.26	703 - 5182	0.002 - 0.0032
Singh and Munjal [40]	Fired clay bricks	✓	✓	✓	60	12	8.24 - 13.34	12.66 - 20.85	2.07 - 5.41	1697 - 4213	0.0026 - 0.0045
Nagarajan et al. [7]	Fired clay bricks	✓	×	✓	12	3	2.67	11.81 - 18.19	1.92 - 2.42	3125 - 3570	0.00085 - 0.00098
Ravula and Subramaniam [8]	Soft clay Bricks	✓	×	✓	6	6	13.9	9.36 - 30	6.2 - 8.1	880	0.0076
Yang et al.[11]	Concrete bricks	✓	×	✓	16	16	8.23	16.24-23.3	4.94 - 6.0	2559-2746	0.00027-0.0030
Kumavat [21]	Vintage clay bricks	✓	×	✓	9	9	3.96	24.98- 28.67	4.61- 5.54	307.2- 369.07	0.015-0.016
Dymiotis and Gutlederer [37]	Burnt clay bricks	✓	✓	✓	38	38	61.02-94.25	2.54-40.43	28.57-60.41	-	-
				Total	518	201	2.67 - 101.7	0.5 - 52.6	2 - 60.41	800 - 22660	0.00018 - 0.017

Table 7. Masonry compressive strength prediction models

Reference	Model	Mean exp./mean predicted.	Stand. dev.	Variance	R^2
Engesser [14]	$f_m = \frac{f_b}{3} + \frac{2f_j}{3}$	0.82	12.53	156.90	0.63
Bröcker [15]	$f_m = 0.68 f_b^{1/2} f_j^{1/2}$	2.14	4.63	21.43	0.13
Mann [16]	$f_m = 0.83 f_b^{0.66} f_j^{0.18}$	1.45	8.02	64.28	0.58
Hendry and Malek [17]	$f_m = 0.317 f_b^{0.531} f_j^{0.208}$	5.62	1.71	2.92	< 0
Dayaratnam [18]	$f_m = 0.275 f_b^{1/2} f_j^{1/2}$	3.46	3.30	10.90	< 0
Kaushik [10]	$f_m = 0.317 f_b^{0.866} f_j^{0.134}$	1.96	7.46	55.63	0.41
Gumasteet al. [19]	$f_m = 0.63 f_b^{0.49} f_j^{0.32}$	2.48	3.90	15.20	0.01
Tensing [20].	$f_m = 0.35 f_b^{0.65} f_j^{0.25}$	3.00	3.93	15.47	< 0
Lumantarna [5]	$f_m = 0.75 f_b^{0.75} f_j^{0.31}$	0.84	16.50	272.16	0.78
Kumavat H. [21].	$f_m = 0.69 f_b^{0.6} f_j^{0.35}$	1.42	8.21	67.48	0.54
Eurocode 6 [13]	$f_m = 0.5 f_b^{0.7} f_j^{0.3}$	1.55	8.36	69.89	0.53
Present study	$f_m = 0.09 f_b^{0.32} f_j^{1.22}\ f_b \leq 20MPa$	1.12	15.8	250	0.91
	$f_m = 1.90 f_b^{0.06} f_j^{0.79}\ f_b > 20MPa$	0.97	31	962	0.87

Table 8. Masonry elastic modulus prediction models

Reference	Model	Mean exp./mean predicted.	Stand. dev.	Variance	R^2
Lumantarna et al. [5]	$E_m = 294 f_m$	1.20	2.43	5886.06	0.41
Paulay and Priestley [22]	$E_m = 750 f_m$	0.45	6.19	38304.79	< 0
Eurocode 6 [13]	$E_m = 1000 f_m$	0.34	8.25	68097.40	< 0
Yang et al. [11]	$E_m = 1513 (f_m)^{1/3}$	1.10	0.77	598.31	0.26
MSJC [23]	$E_m = 700 f_m$	0.48	5.78	33367.73	< 0
Kaushik et al.[10]	$E_m = 550 f_m$	0.62	4.54	20599.46	< 0
Present study	$E_m = 320 f_b^{0.63} f_j^{0.23}$	1.20	2.21	4895.74	0.56

Table 9. Prediction models for masonry peak strain.

Reference	Model	Mean exp./mean predicted.	Stand. dev.	Variance	R^2
Kaushik et al. [10]	$\varepsilon_m = \frac{0.21 f_m}{f_j^{0.21} E_m^{0.7}}$	1.37	2.94×10^{-3}	8.56×10^{-6}	0.42
Lumantarna et al. [5]	$\varepsilon_m = \frac{0.21 f_m}{f_j^{0.25} E_m^{0.7}}$	1.31	3.03×10^{-3}	9.16×10^{-6}	0.47
Zhou et al. [25]	$\varepsilon_m = \frac{0.21 f_m}{f_j^{0.2} E_m^{0.8}}$	2.48	1.70×10^{-3}	2.89×10^{-6}	< 0
Thamboo and Dhanasekar [24]	$\varepsilon_m = \frac{0.0052 f_m}{f_j^{0.05} f_b^{0.29}}$	0.32	1.11×10^{-2}	1.23×10^{-4}	< 0
Yang et al. [11]	$\varepsilon_m = 0.0014\, exp\left(\frac{384 f_m}{E_m}\right)$	0.12	1.33×10^{-1}	1.78×10^{-2}	< 0
Present study	$\varepsilon_m = \frac{0.48 f_m}{f_j^{0.06} E_m^{0.84}}$	1.04	4.19×10^{-3}	1.75×10^{-5}	0.79

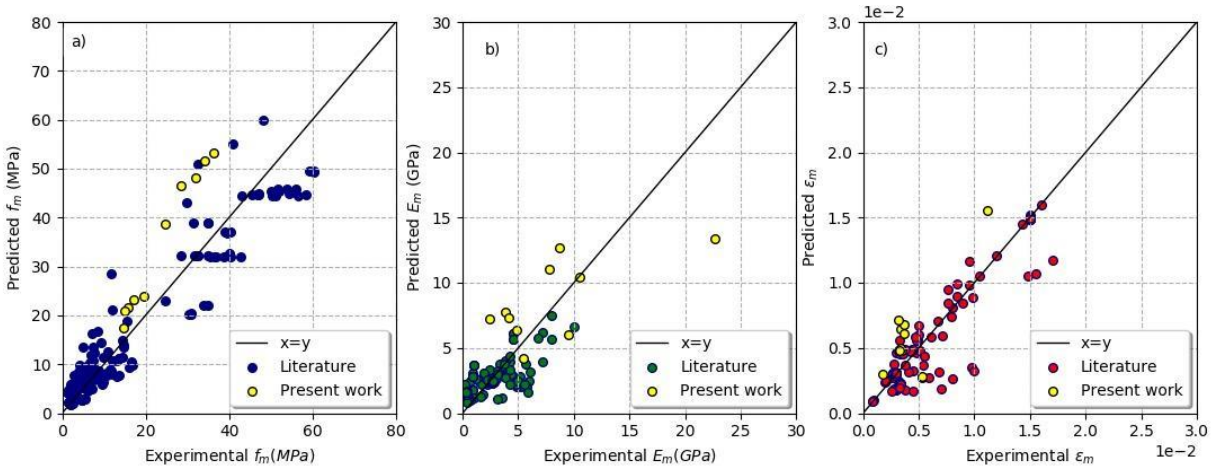

Figure 9 Correlation of proposed model with the experimental database a) masonry compressive strength, b) secant elastic, c) strain at peak stress.

4. 2 Analytical stress-strain relationship

A refined version of the model proposed by Sima et al. [41] was used in this work to model the stress-strain curve of masonry (Figure 10). The model is based on the elastic damage theory, where Hooke's law determines the stress in the elastic phase (Equation 7) and introduces a damage parameter (Equation 8) at the pre-peak stage. The parameters $d_1$and d_2 varies between 0 and 1, describing the damaged state of the material (Equations 9 and 11). The main difficulty of the model lies in the determination of the parameters A, B and C describing the damage in the pre- and post-peak phases. An optimisation approach was adopted to determine these parameters defined in Equations 10 and 12, minimising the differences between experimental and theoretical stress-strain curves. The optimisation allowed for each curve to identify the strain, ε_0 corresponding to the end of the elastic phase as well as the ultimate strain, ε_u which corresponds to zero stress in the descending branch. A total of fifty curves, obtained in this study and retained from the literature [8,10,11,24,39,40], have been optimised, and the strains ε_0 and ε_u were studied as functions of the peak strain, ε_m. The two distinct strains can be expressed by Equations 12 and 13.

Full stress-strain curves and normalised curves for masonry tested in the current work and some plots found in the literature are depicted in Figure 11 with the proposed model, Kaushik et al. [10] and Yang et al. [11] models, respectively. The mechanical properties of all models were obtained using Equations 3, 4 and 6. In figure 11, it can be observed that all models give a satisfactory

prediction until the peak stress of the experimental curve. At post-peak, it can be noted that the model of Yang et al. [11] is more ductile than the model of Kaushik et al. [10]. The proposed model (figure 10) offers a parabolic shape for the post-peak region giving the best fit curve for the experimental data.

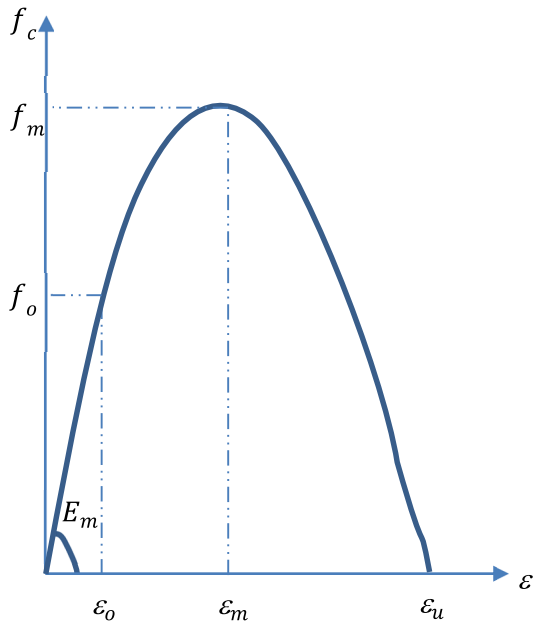

$$f_c = \varepsilon E_m \qquad (\varepsilon \le \varepsilon_0) \tag{7}$$

$$f_c = (1 - d_1) E_m \varepsilon \qquad (\varepsilon_m \le \varepsilon > \varepsilon_0) \tag{8}$$

$$A = \frac{f_c - E_m \varepsilon_0}{E_m [\varepsilon_m e^{\left(\frac{\varepsilon_0 - \varepsilon_m}{\varepsilon_m}\right)} - \varepsilon_0]}, \; d_1 = 1 - \frac{\varepsilon_0 (1 - A)}{\varepsilon - A e^{\left(\frac{\varepsilon_0 - \varepsilon}{\varepsilon_m}\right)}} \tag{9}$$

$$f_c = (1 - d_2) E_m \varepsilon \qquad (\varepsilon > \varepsilon_m) \tag{10}$$

$$\left\langle \begin{matrix} B \\ C \end{matrix} \right\rangle = \frac{\begin{bmatrix} 1 & \varepsilon_m e^{\left(\frac{\varepsilon_0 - \varepsilon_m}{\varepsilon_m}\right)} \\ 1 & \varepsilon_u e^{\left(\frac{\varepsilon_0 - \varepsilon_u}{\varepsilon_m}\right)} \end{bmatrix}^{-1}}{\left\langle \begin{matrix} \frac{f_c}{E_m} \\ 0 \end{matrix} \right\rangle}, \; d_2 = 1 - \frac{B}{\varepsilon - C e^{\left(\frac{\varepsilon_0 - \varepsilon}{\varepsilon_m}\right)}} \tag{11}$$

$$\varepsilon_0 = 0.4279 \varepsilon_m \qquad \varepsilon_m \le 0.006$$

$$\varepsilon_0 = 0.7421 \varepsilon_m \qquad \varepsilon_m > 0.006 \tag{12}$$

$$\varepsilon_u = 2 \varepsilon_m \tag{13}$$

Figure 10 Masonry stress-strain model

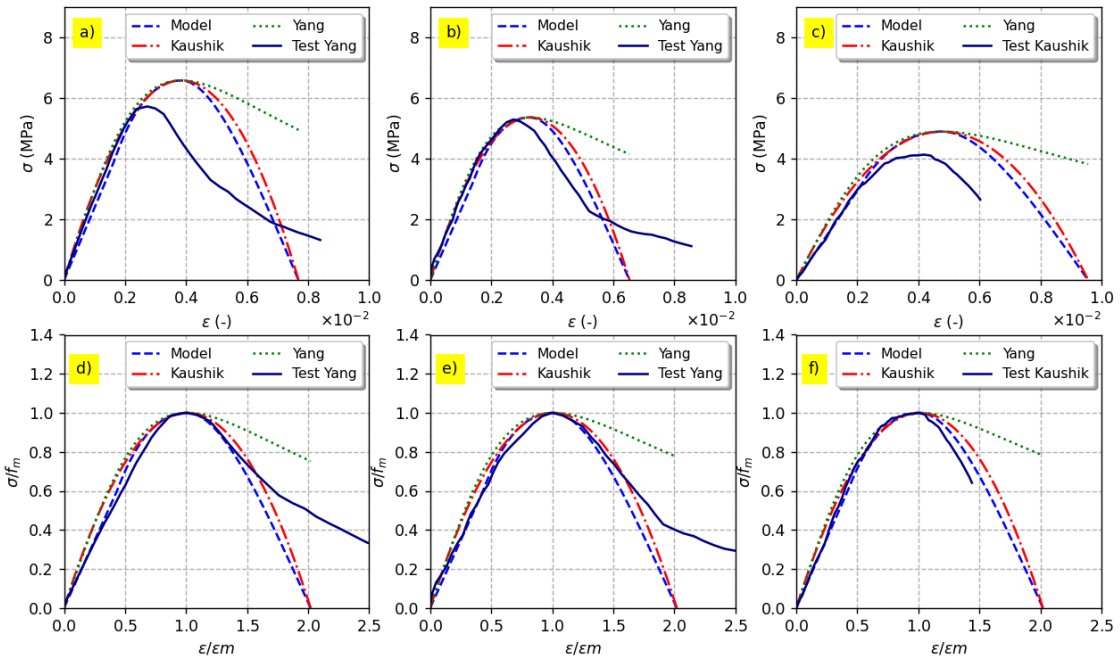

a)

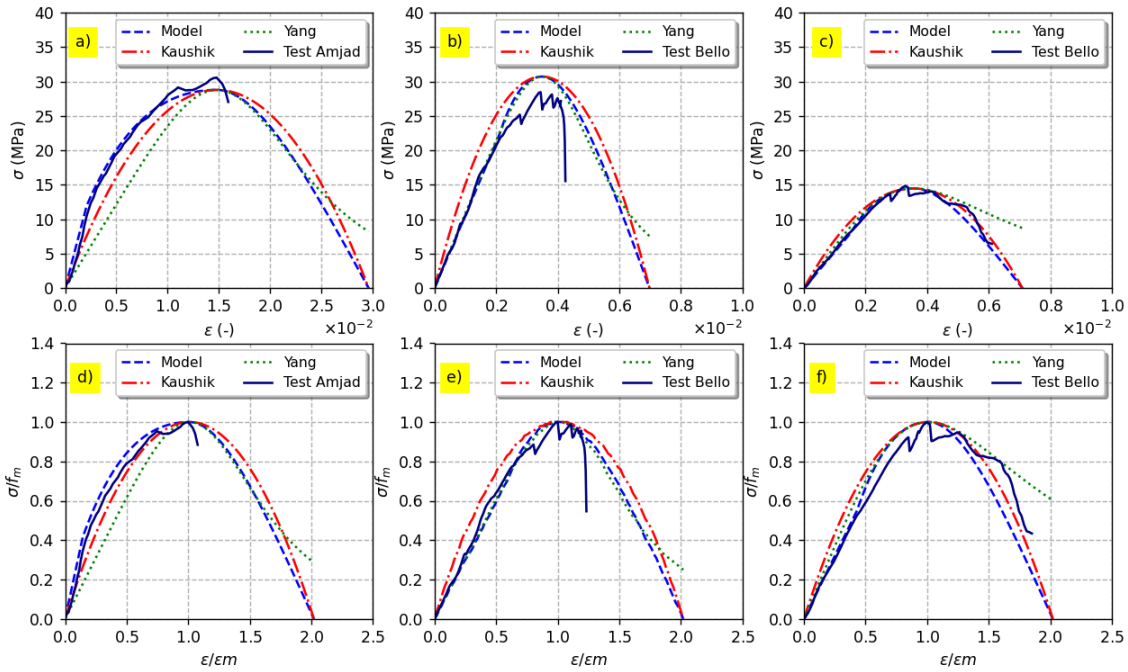

b)

Figure 11 Analytical modelling of full stress-strain curves of experimental tests a) Low compressive strength masonry b) High compressive strength masonry.

5. Conclusion

Characterising the masonry failure mechanism, verifying the DIC approach for measuring the full-field strain, and identifying how the properties of the mortar affect the behaviour of the composite material were the three goals of this work. Under uniaxial monotonic compression loads, two distinct types of fired bricks and five different mortar mixes were tested. The following concluding remarks can be withdrawn in light of the findings:

1 Strains were visualised and measured where strain gauges could not be adapted. A 2D-DIC approach is an effective tool for describing the full-scale compressive behaviour of masonry prisms. However, 2D-DIC is limited to in-plane surface strain measurement.

2 The f_m is determined by the compressive strength of its constituents. Prisms with lower f_b. and f_j. presented lower f_m and vice-versa.

3 The joint mortar composition influences the prism's failure pattern, as prisms with increased cement content were characterised by lateral tensile splitting and spalling, resulting in a brittle failure.

Moreover, prisms with a higher lime content show ductile behaviour with localised strains at the mortar joints.

4 New analytical models were presented to characterise the mechanical properties of masonry prisms using current experimental results and 478 data sets from the literature. The present models have a regression of 0.91 and 0.87 for $f_{m\cdot}$, and 0.56 and 0.79 for $E_{m\cdot}$ and ε_m, respectively.

5 Finally, from current and existing literature on stress-strain curves, a new model was presented to characterise the complete stress-strain behaviour of masonry prisms, where existing analytical models were used to validate its robustness. The model is well adapted for prisms with lime, cement, and lime-cement mortar.

Declaration of Competing interest

The authors declare that they have no known competing financial interests or personal relationships that could have appeared to influence the work reported in this paper.

References

[1] N. Almesfer, D.Y. Dizhur, R. Lumantarna, J.M. Ingham, Material properties of existing unreinforced clay brick masonry buildings in New Zealand, Bulletin of the New Zealand Society for Earthquake Engineering. 47 (2014) 75–96.

[2] D. v Bompa, A.Y. Elghazouli, Compressive behaviour of fired-clay brick and lime mortar masonry components in dry and wet conditions, Mater Struct. 53 (2020) 1–21.

[3] I. Papayianni, V. Pachta, Experimental study on the performance of lime-based grouts used in consolidating historic masonries, Mater Struct. 48 (2015) 2111–2121.

[4] C. Ince, M.A. Carter, M.A. Wilson, The water retaining characteristics of lime mortar, Mater Struct. 48 (2015) 1177–1185.

[5] R. Lumantarna, D.T. Biggs, J.M. Ingham, Uniaxial compressive strength and stiffness of field-extracted and laboratory-constructed masonry prisms, Journal of Materials in Civil Engineering. 26 (2014) 567–575.

[6] W.S. McNary, D.P. Abrams, Mechanics of masonry in compression, Journal of Structural Engineering. 111 (1985) 857–870.

[7] T. Nagarajan, S. Viswanathan, S. Ravi, V. Srinivas, P. Narayanan, Experimental approach to investigate the behaviour of brick masonry for different mortar ratios, in: International Conference on Advances in Engineering and Technology, Singapore, 2014: pp. 586–592.

[8] M.B. Ravula, K.V.L. Subramaniam, Experimental investigation of compressive failure in masonry brick assemblages made with soft brick, Mater Struct. 50 (2017) 1–11.

[9] N.N. Thaickavil, J. Thomas, Behaviour and strength assessment of masonry prisms, Case Studies in Construction Materials. 8 (2018) 23–38.

[10] H.B. Kaushik, D.C. Rai, S.K. Jain, Stress-strain characteristics of clay brick masonry under uniaxial compression, Journal of Materials in Civil Engineering. 19 (2007) 728–739.

[11] K.-H. Yang, Y. Lee, Y.-H. Hwang, A stress-strain model for brick prism under uniaxial compression, Advances in Civil Engineering. 2019 (2019).

[12] A. Drougkas, P. Roca, C. Molins, Numerical prediction of the behavior, strength and elasticity of masonry in compression, Eng Struct. 90 (2015) 15–28.

[13] B. Standard, Eurocode 6—Design of masonry structures—, British Standard Institution. London. (2005).

[14] F. Engesser, Über weitgespannte wölbbrücken, Zeitschrift Für Architekturs Und Ingenieurwesen. 53 (1907) 403–440.

[15] O. Bröcker, Die auswertung von tragfähigkeitsversuchen an gemauerten wänden, Betonstein-Zeitung. 10 (1963) 19–21.

[16] W. Mann, Statistical evaluation of tests on masonry by potential functions, in: Sixth International Brick Masonry Conference, 1982.

[17] A.W. Hendry, M.H. Malek, Characteristic compressive strength of brickwork walls from collected test results, MASONRY INT. Masonry Int. (1986) 15.

[18] P. Dayaratnam, Brick and reinforced brick structures, South Asia Books, 1987.

[19] K.S. Gumaste, K.S. Nanjunda Rao, B. v Venkatarama Reddy, K.S. Jagadish, Strength and elasticity of brick masonry prisms and wallettes under compression, Mater Struct. 40 (2007) 241–253.

[20] D. Tensing, Experimental study on axial compressive strength and elastic modulus of the clay and fly ash brick masonry, Journal of Civil Engineering and Construction Technology. 4 (2013) 134–141.

[21] H.R. Kumavat, An experimental investigation of mechanical properties in clay brick masonry by partial replacement of fine aggregate with clay brick waste, Journal of The Institution of Engineers (India): Series A. 97 (2016) 199–204.

[22] T. Paulay, M.J.N. Priestley, Seismic design of reinforced concrete and masonry buildings, (1992).

[23] MSJC, Building Code Requirements for Masonry Structures (TMS 402-xx/ACI 530-xx/ ASCE 5-xx), 2011.

[24] J.A. Thamboo, M. Dhanasekar, Correlation between the performance of solid masonry prisms and wallettes under compression, Journal of Building Engineering. 22 (2019) 429–438.

[25] Q. Zhou, F. Wang, F. Zhu, X. Yang, Stress–strain model for hollow concrete block masonry under uniaxial compression, Mater Struct. 50 (2017) 1–12.

[26] B.D. Ewing, M.J. Kowalsky, Compressive behavior of unconfined and confined clay brick masonry, Journal of Structural Engineering. 130 (2004) 650–661.

[27] D.J. Carreira, K.-H. Chu, Stress-strain relationship for plain concrete in compression, in: Journal Proceedings, 1985: pp. 797–804.

[28] B. Pan, K. Qian, H. Xie, A. Asundi, Two-dimensional digital image correlation for in-plane displacement and strain measurement: a review, Meas Sci Technol. 20 (2009) 62001. https://doi.org/10.1088/0957-0233/20/6/062001.

[29] R. Ghorbani, F. Matta, M.A. Sutton, Full-field deformation measurement and crack mapping on confined masonry walls using digital image correlation, Exp Mech. 55 (2015) 227–243.

[30] J.-F. Destrebecq, E. Toussaint, E. Ferrier, Analysis of cracks and deformations in a full scale reinforced concrete beam using a digital image correlation technique, Exp Mech. 51 (2011) 879–890.

[31] I. Bello, G. Wardeh, B. Gonzalez-Fonteboa, F. Martinez-Abella, Strain measurement of construction materials with digital image correlation, in 2021 Fib Symposium of Concrete Structures: New Trends for Eco-Efficiency and Performance, pp. 1529–1538. https://www.fib-international.org/publications/fib-proceedings/i-fib-i-symposium-in-lisbon,-portugal-2021-proceedings-em-pdf-em-detail.html.

[32] S.-H. Tung, M.-H. Shih, W.-P. Sung, Development of digital image correlation method to analyse crack variations of masonry wall, Sadhana. 33 (2008) 767–779.

[33] EN-P18-452, Concretes - Measuring the flow time of concretes and mortars using a workabilitymeter, European Standard. ST(norme) (2017) P18--452.

[34] G. Sarangapani, B. v Venkatarama Reddy, K.S. Jagadish, Brick-mortar bond and masonry compressive strength, Journal of Materials in Civil Engineering. 17 (2005) 229–237.

[35] S. Harenberg, M. Pahn, V. Malárics- Pfaff, F. Dehn, A. Caggiano, D.S. Schicchi, S. Yang, E. Koenders, Digital image correlation strain measurement of ultra- high- performance concrete- prisms under static and cyclic bending- tensile stress, Structural Concrete. 20 (2019) 1220–1230.

[36] GOM Metrology, GOM correlate software, Https://Www.Gom.Com/Index.Html. (n.d.).

[37] C. Dymiotis, B.M. Gutlederer, Allowing for uncertainties in the modelling of masonry compressive strength, Constr Build Mater. 16 (2007) 1385–1393.

[38] N. Domede, G. Pons, A. Sellier, Y. Fritih, Mechanical behaviour of ancient masonry, Mater Struct. 42 (2009) 123–133.

[39] A.J. Aref, K.M. Dolatshahi, A three-dimensional cyclic meso-scale numerical procedure for simulation of unreinforced masonry structures, Comput Struct. 120 (2013) 9–23.

[40] S.B. Singh, P. Munjal, Bond strength and compressive stress-strain characteristics of brick masonry, Journal of Building Engineering. 9 (2017) 10–16.

[41] J.F. Sima, P. Roca, C. Molins, Cyclic constitutive model for concrete, Eng Struct. 30 (2008) 695–706.